Optical control of a metastable phase in the charge density wave Mott insulator $1T$-TaS_2 investigated using time- and angle-resolved photoemission spectroscopy

Tanusree Saha,[1,2,*] Arindam Pramanik,[3,4] Rokaya Osama,[2] Fabio Frassetto,[5] Damjan Krizmancic,[6] Luca Poletto,[5] Arun Ravindran,[2] Barbara Ressel,[2] Primož Rebernik Ribič,[7] and Giovanni De Ninno[2,7]

[1]*Faculty of Physics, University of Duisburg-Essen, 47057 Duisburg, Germany*

[2]*Laboratory of Quantum Optics, University of Nova Gorica, 5270 Ajdovščina, Slovenia*

[3]*Academic Centre for Materials and Nanotechnology, AGH University of Krakow, Al. Mickiewicza 30, 30-059 Krakow, Poland*

[4]*Department of Theoretical Physics, Tata Institute of Fundamental Research, Mumbai 400005, India*

[5]*CNR-Institute of Photonics and Nanotechnologies (CNR-IFN), 35131 Padova, Italy*

[6]*CNR-IOM, Strada Statale 14 km 163.5, 34149 Basovizza (TS), Italy*

[7]*Elettra Sincrotrone Trieste, Strada Statale 14 km 163.5, 34149 Trieste, Italy*

(Received 29 May 2025; revised 20 October 2025; accepted 19 November 2025; published 6 January 2026; corrected 13 February 2026)

Light-induced metastable phases are exotic, long-lived out-of-equilibrium states of matter. Optical control offers a powerful approach to engineering these phases, enabling dynamic tuning of their electronic and structural properties. Using time- and angle-resolved photoemission spectroscopy, we investigate the emergence of a metastable phase induced by a strong infrared pump in the charge-density-wave (CDW)-Mott insulator $1T$-TaS_2. Furthermore, we demonstrate how its properties can be optically manipulated by varying the photoexcitation strength. A long-lived stabilization of the renormalized electronic band structure serves as a signature of the metastable phase. It displays a relaxed periodic lattice distortion (PLD) and primarily lattice-driven dynamics. The emergence of a new dispersive band in the vicinity of the Hubbard bands reveals the formation of a novel band structure unique to the metastable phase. Our pump-fluence-dependent studies reveal a threshold (incident) fluence $F_C \sim 1.3\text{mJ/cm}^2$ for inducing the metastable phase, above which the band renormalization continuously evolves with increasing fluence. For $F \leqslant 3.4\ \text{mJ/cm}^2$, stronger photoexcitation progressively drives the phase to higher energies, accompanied by a more relaxed PLD and reduced CDW amplitude. The properties of the metastable phase are strongly influenced by the transient dynamics at each fluence, and the associated fast timescales suggest that the intrinsic CDW amplitude mode remains unaffected by optical manipulation. These findings highlight the potential of optical control in tuning the properties of metastable phases in quantum materials, offering new insights into the manipulation of CDW systems and paving the way for future investigations in nonequilibrium phase engineering.

DOI: 10.1103/gz2s-685y

I. INTRODUCTION

Ultrafast light-matter interactions can manipulate quantum materials on femtosecond timescales, leading to novel electronic, magnetic, and structural properties [1,2]. They can give rise to various exotic phenomena, such as light-induced superconductivity [3–5], nonlinear phononics [6], magnetic field from optically-driven phonons [7], terahertz field-induced ferroelectricity [8], and Floquet-Bloch states in topological insulators [9,10]. Multiple nonthermal pathways have been established for active manipulation of materials via transient modification to the free energy landscape, ultrafast heating, and Floquet engineering [11]. For example, these control schemes govern quasiparticle recombination and gap formation in cuprates on femtosecond to picosecond timescales [12] and coherent control of structural phase transitions [13]. In materials, like layered transition-metal dichalcogenides, with competing microscopic interactions, photoexcitation by ultrashort light pulses can induce 'hidden' phases with properties that are otherwise inaccessible under thermal equilibrium conditions [14–17].

Some of the light-induced hidden phases can be very long lived [8,18–20] or can persist indefinitely under suitable environmental conditions [21–25]. Important examples include optical switching to hidden metallic states in VO_2 [18], Mott materials [26], and strain engineered manganite films [21], and metastable photo-induced superconductivity in the fulleride K_3C_{60} far above the superconducting T_C in equilibrium [27]. These phases have recently gained significant attention as a growing research area in condensed matter physics. Their distinctive properties make them valuable for applications in optoelectronics, as well as energy storage and conversion in thermoelectric devices. Furthermore, manipulating the properties of metastable phases is at the frontier of material science as it opens pathways to dynamically engineer quantum materials. These exceptional phases can be

*Contact author: tanusree.saha@uni-due.de

externally controlled via optical, thermal, mechanical means, and via application of electric fields (e.g., ferroelectrics).

One of the prominent metastable phases emerging in correlated systems is the metallic hidden phase of $1T$-TaS_2. Due to its intriguing properties, its origin and formation mechanism are extensively studied using transport measurements [28,29], microscopy [30–32], diffraction [33], and pump-probe spectroscopy [22,31]. It consists in an insulator-to-metal transition with a substantial drop in electrical resistivity. Such a state can persist indefinitely, with stable switching achieved either by optical pulses or through joule heating [22,28,30,31,33–38]. Furthermore, a transient imbalance in the electron-hole populations has been suggested as a driver of the hidden state [22]. The atomic configuration in the hidden phase has been studied [31,33–35] and the origin of metallicity is under debate [22,33,35,39].

In thermal equilibrium, $1T$-TaS_2 exhibits a variety of ground states due to the interplay between Coulomb repulsion, charge density wave ordering, and interlayer coupling [40–45]. At very high temperatures, it is metallic having an undistorted hexagonal lattice structure. It undergoes successive first-order phase transitions upon cooling. From the metallic phase, $1T$-TaS_2 enters an incommensurate IC-CDW phase at 550 K, and then to a nearly commensurate NC-CDW phase at 350 K. It further undergoes a phase transition to a commensurate C-CDW phase at $T_{\mathrm{CDW}} = 180$ K. In the CDW phases, Star-of-David (SOD) clusters form the fundamental units describing the lattice. The SOD comprises 12 Ta atoms (6 atoms in each ring) that are radially displaced inwards towards the central 13th Ta atom within a layer, see Fig. 1(a). Due to the $\sqrt{13} \times \sqrt{13}$ superlattice formation [unit cell shown by red dashed lines in Fig. 1(a) (left)], the Ta $5d$ valence band is split into three subband manifolds, giving rise to narrow half-filled band at the Fermi level E_F. This flat band is susceptible to a Mott-Hubbard transition [44,46], which leads to its separation into two distinct spectral features: the Lower and Upper Hubbard bands. The C-CDW phase has a long-range intralayer electronic and lattice order. However, the intermediate NC-CDW and trigonal CDW phases consist of periodic arrays of SOD clusters separated by metallic regions without this order [45,47]. In addition, the interlayer stacking configuration of the CDW reconstructed layers is suspected to strongly affect the electronic states near E_F, putting the origin of the insulating phase into debate [34,39,48–50]. As a material that hosts multiple phases, $1T$-TaS_2 provides a rich platform for studying the quench dynamics of electronic and lattice ordering on ultrafast timescales [51–60].

The metastable phase in $1T$-TaS_2 has been extensively studied, yet the separate dynamics of electron correlations (Mott) and CDW order in this phase remain unexplored—an important question in materials with coexisting phases. Using time- and angle-resolved photoemission spectroscopy (tr-ARPES), we decouple these dynamics through band-selective measurements along different k directions in the Brillouin zone. Optical control of metastable phases enables dynamical tuning of microscopic interactions, potentially leading to new quantum states. While single-shot transient reflectivity studies [37] have demonstrated photoexcitation-driven tuning of the metastable phase, they lack sensitivity to electronic band structure, precluding direct insight into CDW dynamics

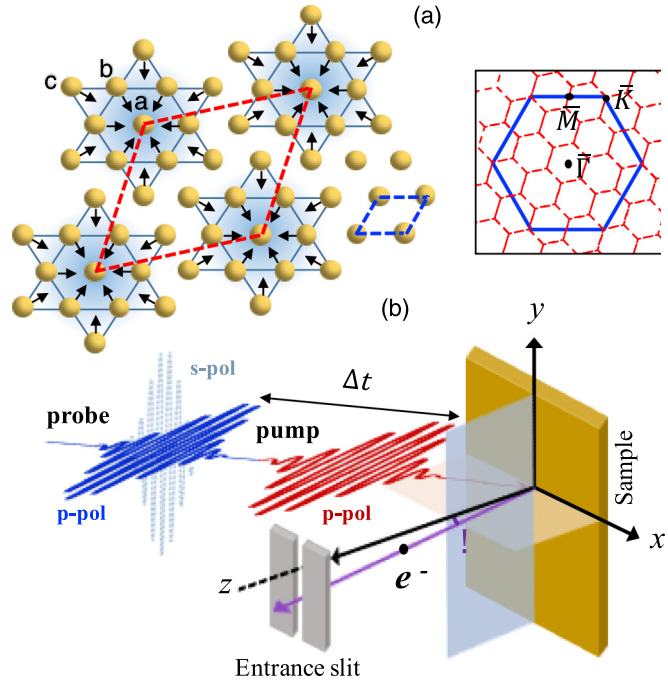

FIG. 1. Structure and geometry: (a) (Left) In-plane structural distortion in the C-CDW phase of $1T$-TaS_2 produces Star-of-David clusters having inequivalent (a, b, c) Ta atoms. Red and blue dashed lines indicate the real space unit cells in the C-CDW and unreconstructed phases, respectively. The arrows indicate the radial displacement of the Ta atoms from the inner and outer rings towards the central atom. (Right) Reciprocal space Brillouin zone in the unreconstructed (blue) and distorted (red) phases with high-symmetry points $\bar{\Gamma}, \bar{M}, \bar{K}$. (b) Schematic of the pump-probe experimental geometry for the time-resolved ARPES measurements. Δt is the pump-probe delay, θ is the photoelectron emission angle in the yz plane w.r.t. z axis.

independent of electron correlations. Similarly, a recent time-resolved ARPES study [38] revealed pump-fluence-dependent control of the Lower Hubbard band (LHB). However, our findings indicate that under nonequilibrium conditions, the LHB dynamics remain intertwined with another band (details in the text) that exhibits pronounced spectral weight. As a consequence, the time-dependent spectral evolution of the LHB does not reveal precise optical control over the metastable phase, nor does it clearly separate CDW-related and Mott-related features. To address this scenario, an energy band decoupled from intertwined spectral features must be examined. We accomplish this by studying the pump fluence-dependent dynamics of a CDW-originated subband at 1 eV binding energy using tr-ARPES across a broad range of photoexcitation density.

Upon strong infrared optical excitation, we find a pronounced and persistent (for several picoseconds) renormalization of the band structure along $\bar{M} \rightarrow \bar{K}$ (see Fig. 1(a) for high-symmetry k points in the Brillouin zone), indicating the formation of a metastable phase. This phase is characterized by a relaxed periodic lattice distortion (PLD) and a reduced CDW amplitude. Temperature-dependent modification of band structure in equilibrium reveal that this metastable phase is a novel phase that arises only under

nonequilibrium conditions. Furthermore, we identify a new dispersive band above E_F that characterizes the electronic structure of the metastable phase. This feature may suggest a coexistence of metallic and insulating phases with domainlike C-CDW configuration; alternatively, it more likely reflects the emergence of a novel band structure intrinsic to the electronic and lattice order of the metastable phase. Next, our fluence-dependent studies in the range of 0.5 – 3.5 mJ/cm^2 identify a critical (incident) fluence, $F_C \sim 1.3$ mJ/cm^2, or, equilvalently an absorbed critical fluence $F_C^{ab} \sim 0.7$ mJ/cm^2, required for the emergence of the metastable phase. Above this threshold, the continuous evolution of the band renormalization with increasing fluence (along $\bar{M} \rightarrow \bar{K}$) reflects a modification in the properties of the metastable phase. As fluence increases, a larger bandwidth and bandshift towards higher energies are observed over very long timescales. These indicate enhanced relaxation of the PLD, driving the system towards progressively higher energy states. The characteristics of the metastable phase are strongly coupled to transient modifications of lattice distortion at each fluence. The associated transient timescale of ∼200 fs remains independent of fluence, suggesting that the intrinsic CDW amplitude mode remains unaffected by optical manipulation. Our findings demonstrate that optical excitation provides a viable pathway for controlling the properties of metastable phases in complex solids, with implications for future functional materials.

II. EXPERIMENTAL DETAILS

Time- and angle-resolved photoemission experiments were performed at the CITIUS high-harmonic generation (HHG) light source [61]. The source is driven by a mode-locked Ti:Sapphire laser delivering 800-nm pulses, with a time duration of 40 fs at 5 kHz repetition rate. The major part of the driving laser intensity was used to generate extreme-ultraviolet probe pulses through HHG, with Ar as the generating medium, and the remaining intensity was used for the pump pulses. All discussed fluences refer to the incident fluence (in mJ/cm^2), unless stated otherwise. This is determined from the expression $2E_p/(\pi w^2)$, where E_p is the energy per pulse and w is the beam waist at the sample position. The photon energy of the probe pulse was selected by a monochromator grating with off-plane geometry, which preserved the pulse duration [62]. The fundamental frequency of the laser, $h\nu = 1.55$ eV, was used as the pump pulse energy. A photon energy $h\nu$∼20 eV was selected for the probe pulses due to higher photoionization cross section of the Ta 5d bands and a high photon flux. Both $\boldsymbol{p}$ and $\boldsymbol{s}$ polarizations of the probe were used to selectively probe different Ta 5d subbands, while the pump was always set to $\boldsymbol{p}$ polarization. A schematic of the pump-probe experimental geometry is shown in Fig. 1(b). The energy and time resolution of the experiment were 150 meV and 50 fs, respectively. The ultrahigh vaccum setup at CITIUS is equipped with an R3000 hemispherical electron analyzer from VG Scienta. All the time-resolved ARPES experiments were performed at a sample temperature of 100 K $< T_{\mathrm{CDW}}$, where the lifetime of the metastable phase is shorter than the repetition time (0.2 ms ↔ 5 kHz) of the laser source, allowing its investigation using a stroboscopic pump-probe scheme. A closed-cycle He cryostat was used to control the sample temperature. High-quality single crystals of 1T-TaS_2 were purchased from HQ Graphene. The trARPES experiments were performed at a base pressure < 1x10^{-10} mbar.

For $\boldsymbol{p}$-polarized pump at $\lambda = 800$ nm, the absorption in 1T-TaS_2 is 56%. This can be obtained from Fresnel equations that describe the reflection and transmission/absorption of light incident on an interface between two different optical media. The reflectance, R, is given by $|\frac{\tilde{n}_2 \cos\theta_i - n_1 \cos\theta_t}{\tilde{n}_2 \cos\theta_i + n_1 \cos\theta_t}|^2$, with $\cos\theta_t = \sqrt{1 - (\frac{n_1}{\tilde{n}_2}\sin\theta_i)^2}$ (Snell's law), and consequently, the absorption is $1 - R$. Our experimental parameters are $\tilde{n}_2$ (1T-TaS_2) $= n + ik$, where $n = 3.2$ and $k = 2.9$, n_1 (air) $= 1$, and $\theta_i = 36^\circ$. Here, n_1, $\tilde{n}_2$ are the refractive indices of the media and θ_i, θ_t are the angles of incidence and refraction, respectively.

III. RESULTS

A. Band-selective dynamics probing CDW and Mott physics in the light-induced metastable phase

In the equilibrium band structure of 1T-TaS_2 below T_{CDW} [44,46], the Ta 5d subbands lying at binding energies of ∼1 and ∼0.5 eV are predominantly of CDW origin, whereas the states near E_F at ∼0.2 eV are strongly influenced by electron correlations. The renormalization of the higher-energy subbands can therefore be recognized as a spectroscopic indicator of the CDW-related electron and lattice dynamics. At the same time, the evolution of low energy flat bands—the lower and upper Hubbard bands—serves as a signature of the Mott dynamics.

1. Band renormalization capturing CDW dynamics

Among the higher-energy subbands, we select the band at 1 eV along $\bar{M} \rightarrow \bar{K}$, because of its distinct spectral features [55] and prominent pump-induced changes [53]. In the following, we refer to this band as the B_2 band. Figure 2 shows the time evolution of B_2 band after strong photoexcitation with fluence ∼3.7 mJ/cm^2. The ARPES snapshots at various time delays in Fig. 2(a) exhibit distinct signatures of band renormalization. For a detailed analysis of the band dynamics, the E vs $k_\parallel$ dispersion at different pump-probe delays were extracted from the corresponding ARPES spectra, as plotted in Fig. 2(b). For the ARPES spectra at each time delay, we determine the peak energy position of the energy distribution curve (EDC) at each $k_\parallel$. Plotting these peak energies versus their corresponding $k_\parallel$ values yields the dispersion. The renormalization is characterized by variations in bandwidth and bandshift. Here, bandwidth refers to the energy difference between the band minimum at $k_\parallel = 0$ (at $\bar{M}$) and band maximum at $k_\parallel > 0.2$ Å^{-1} (towards $\bar{K}$), whereas bandshift refers to the change in energy at $k_\parallel = 0$. A pronounced increase in the bandwidth and substantial bandshift towards lower binding energy is observed at 300 fs, after which the renormalization starts to recover. To further quantify these changes, the time evolution of band parameters is presented in Figs. 2(c) and 2(d). The initial increase in band parameters occurs on a ∼200 fs timescale, corresponding to the CDW amplitude mode (structural timescale) [63,64] in 1T-TaS_2 at temperatures below T_{CDW}. As the significantly altered band structure begins to recover, a long-lived state emerges beyond ∼700 fs.

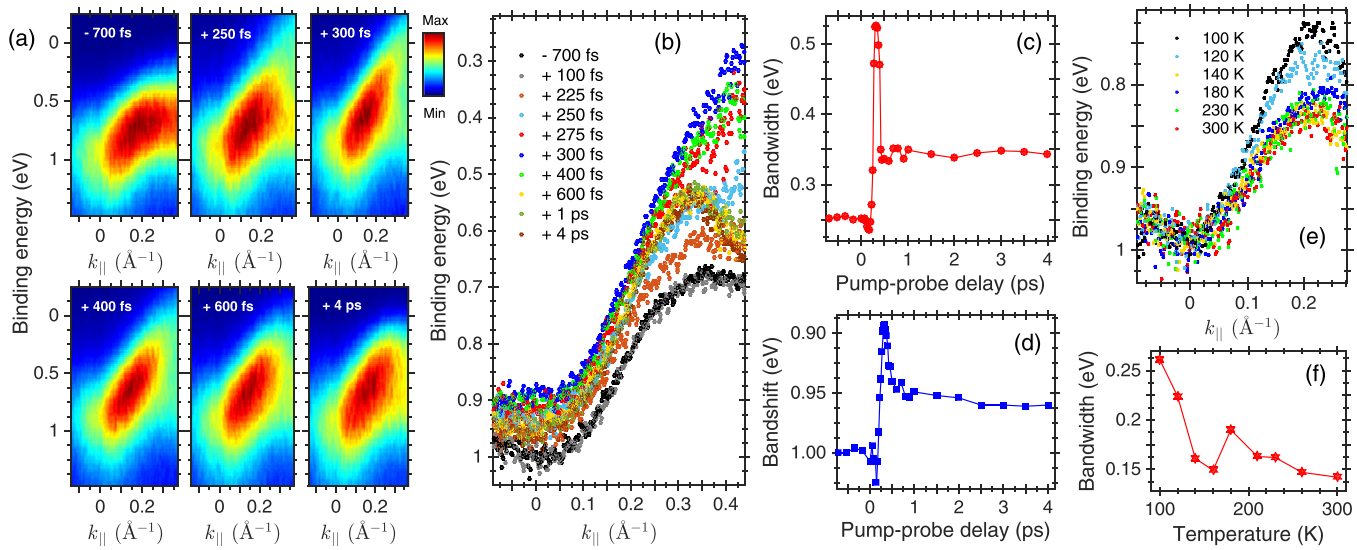

FIG. 2. Renormalization of B_2 band along $\bar{K} \leftarrow \bar{M} \rightarrow \bar{K}$ ($\bar{M}$ at $k_{\parallel} = 0$): (a) Time-resolved ARPES spectra in the C-CDW phase of $1T$-TaS_2, measured by ***s***-polarized probe pulses. The sample temperature is 100 K and incident pump fluence is 3.7 mJ/cm^2. (b) E vs $k_{\parallel}$ dispersion at various pump-probe delays obtained from the peak position of the EDCs at each $k_{\parallel}$ from corresponding ARPES spectra in (a). (c) Bandwidth (energy difference between band minimum at $k_{\parallel} = 0$ and band maximum at $k_{\parallel} > 0.2$ Å^{-1}) as a function of time. (d) Evolution of bandshift (energy shift at $k_{\parallel} = 0$) with time. The bandwidth and bandshift values are accurate within ± 8 and ± 4 meV, respectively. (e) Temperature-dependent band dispersion in equilibrium. (f) Bandwidth as a function of temperature obtained from (e), accurate within ± 10 meV.

This is marked by the saturation of the bandwidth at a larger value and the bandshift at a lower binding energy relative to the equilibrium values. It persists for several hundreds of picoseconds, indicating the emergence of a metastable phase.

Our interpretation of the observed phenomena is as follows. Upon photoexcitation, a fraction of the electronic charge density migrates from the central Ta atom towards the outer ring of SOD clusters [44]. In response, this causes a repositioning of the atoms and subsequent relaxation of the clusters. The transient changes in band parameters until ∼350 fs can be attributed to an increased hybridization among the clusters (mainly, the outer ring of SODs). In fact, the structural timescale characterizing the transient changes emphasizes that the induced dynamics are mainly lattice driven. The renormalized band structure in the metastable phase indicates that the PLD remains sufficiently relaxed before the system can fully revert back to its ground state. This suggests that the redistributed electronic density within a cluster has not recovered. This can be clearly noted from the low spectral intensity of the LHB at 1.6 ps in Fig. 3(b), since the DOS near E_F is dominated by electronic states close to the central atom [44]. From our temperature-dependent ARPES results in equilibrium, it can be argued that the metastable phase is different from any of the high-temperature equilibrium phases driven by lattice heating. The evolution of the occupied band structure in equilibrium along $\bar{M} \rightarrow \bar{K}$ as a function of temperature during the heating cycle (100 → 300 K) is shown in Fig. 2(e) and the temperature-dependent bandwidth is plotted in Fig. 2(f). Momentum-resolved EDC stacks at different temperatures extracted from the corresponding ARPES spectra are shown in the Supplemental Material [65]. We observe that the bandwidth decreases with temperature, which contrasts with our observations for the metastable phase in Figs. 2(b) and 2(c). Above 140 K, the evolution is minimal, with only a small abrupt change near T_{CDW}, see Fig. 2(f). These observations indicate that the metastable phase is not simply a consequence of the rise in lattice temperature. Our findings show that this phase is a unique new phase induced in photoexcited $1T$-TaS_2, one that cannot be realized under equilibrium conditions.

2. Renormalization dynamics of Mott-Hubbard bands

Having established the CDW dynamics in the metastable phase, we now turn to the modification of Mott physics in this long-lived state by tracking the time evolution of the low-energy Hubbard bands. Based on symmetry-based selection rules in photoemission, the light polarization is tuned to target orbitals of specific symmetry [66]: ***p***-polarized probe pulses reveal the lower Hubbard band, whereas ***s***-polarized pulses capture the upper Hubbard band (UHB). Figure 3 presents the LHB and UHB renormalization dynamics along $\bar{\Gamma} \rightarrow \bar{M}$ [see Fig. 1(a)] at a high pump fluence of 4.6 mJ/cm^2. We can distinctly observe LHB at ∼0.2 eV (equilibrium binding energy; blue arrow) at −800 fs and transiently populated UHB at −0.2 eV at 250 fs (green arrow) in the time-resolved ARPES spectra in Figs. 3(a) (left) and 3(c) (right), respectively. At 250 fs, with the LHB shifted to 0.4 eV in Fig. 3(a) (right), a prominent feature of the ARPES spectrum is the formation of a new band (red arrow) above E_F. In the following, we refer to it as the M band. It exhibits a dispersive feature with its minimum located at $\bar{\Gamma}$ [57]. Although the M band was observed within 300 fs and its band structure was well resolved at ≈300 fs in our previous work [57], its dynamics were not explored. The present study focuses on a comprehensive analysis of its emergence, and time-dependent band evolution, with particu-

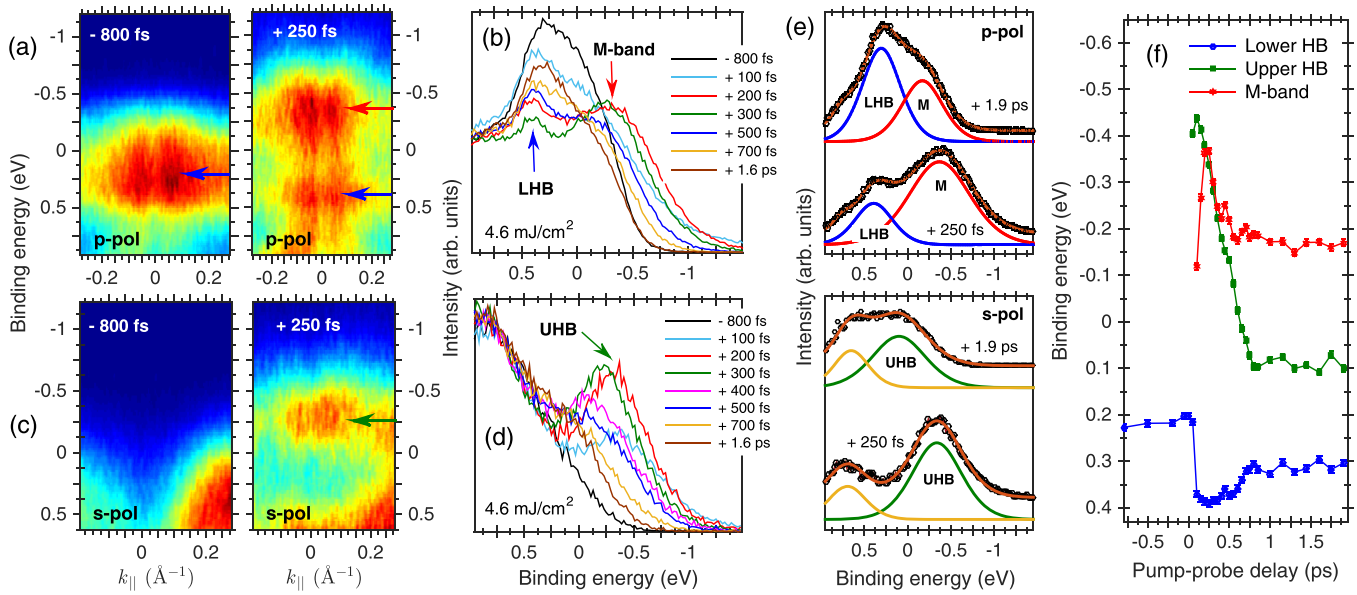

FIG. 3. Renormalization of Lower and Upper Hubbard bands along $\bar{M} \leftarrow \bar{\Gamma} \rightarrow \bar{M}$ ($\bar{\Gamma}$ at $k_\parallel = 0$): (***p***-polarized probe) (a) ARPES spectra in equilibrium (left) and at 250 fs after photoexcitation (right). In addition to LHB (blue arrow), photoexcitation gives rise to a prominent, intense feature above E_F, namely, the M band (red arrow). (b) $k_\parallel$-integrated [± 0.05 Å^{-1} in (a)] spectral intensity at various pump-probe delays, showing the evolution of LHB and M band. (***s***-polarized probe) (c) ARPES spectra in equilibrium (left) and at 250 fs (right). UHB (green arrow) can be distinctly observed above E_F. (d) $k_\parallel$-integrated [± 0.02 Å^{-1} in (c)] spectral intensity at various pump-probe delays, showing the evolution of UHB. (e) Peak fitting of the $k_\parallel$-integrated intensity at 250 fs and 1.9 ps with (top panel) ***p***- and (bottom panel) ***s***-polarized probe. (f) Time-dependent evolution of the Hubbard bands and M band. The incident pump fluence is 4.6 mJ/cm^2. Data points are shown with an error bar of ± 5 meV, representing the fitting uncertainty.

lar emphasis on its behavior in the metastable phase. The time evolution of $k_\parallel$-integrated spectral intensity of LHB, M band and UHB are plotted in Figs. 3(b) and 3(d), respectively. The $k_\parallel$-integration range are ± 0.05 and ± 0.02 Å^{-1} around $\bar{\Gamma}$-point for ***p***- and ***s***-polarized data, respectively. In Fig. 3(b), the M band emerges within 100 fs after photoexcitation and persists alongside the LHB at later time delays. While in Fig. 3(d), an intensity gain above E_F within 100 fs marks the UHB, which remains prominent at longer times.

To closely monitor the time-dependent dynamics of the three bands, the peak energy positions of these bands, displayed in Fig. 3(f), were determined by fitting the EDCs in Figs. 3(b) and 3(d) at each time delay. For each raw EDC, an appropriate background lineshape (Tougaard, in the present case) was subtracted, and the resulting EDC was fitted with one or more peaks using a Lorentzian–Gaussian (40–60) profile. The Gaussian contribution dominates, as the energy broadening due to the experimental resolution exceeds the intrinsic lifetime broadening. The obtained fitting parameters (energy) were then plotted as a function of time. No additional data processing was applied. A few of the fitted spectra are shown in Fig. 3(e). Because the spectral intensity of the UHB and M band decreases over time, it becomes challenging to clearly identify these features beyond a few 100 fs. Therefore, a sufficiently high pump fluence was selected to ensure their distinct resolution on the picosecond timescale. This is shown in Fig. 3(e), where the fitted EDCs at 1.9 ps clearly resolve the LHB and M band (top panel) and a prominent UHB (bottom panel), similar to the corresponding EDCs at 350 fs. The yellow peak at $\sim$0.6 eV in Fig. 3(e) (bottom panel) arises from the S $3p$ band located at higher binding energy. Although our energy window does not capture the full S $3p$ band, background subtraction during the fitting procedure produces a peak at this energy, which has no relevance to the present study.

Some of the key characteristics of the bands are observed. Within 100–150 fs, the LHB shifts from 0.2 eV to a higher binding energy, then gradually recovers, stabilizing at 0.3 eV after $\sim$700 fs. Simultaneously, the UHB undergoes a continuous shift from -0.4 eV to higher binding energy after 100 fs, eventually reaching a plateau at 0.1 eV beyond 700 fs. These indicate a reduction of the Mott gap, characterized by both fast (a few 100 fs) and slow (several ps) timescales. The gap ultimately saturates at 0.2 eV, smaller than its equilibrium value of 0.4 eV. Our results confirm the presence of the Mott insulator phase, indicative of strong electron correlations, even at longer times when the material has transitioned into the metastable phase. The dynamics of Hubbard bands within 300–400 fs are in agreement with our recent work [57]. Although interlayer dimerization of the S–Ta–S layers has been widely considered a potential origin of the band gap, our observations—suppression of the LHB intensity and simultaneous reduction of the band gap with time—point towards a possible Mott-insulating scenario. On the other hand, the M band exhibits a distinct behavior: starting at -0.1 eV at 50 fs, it initially shifts to a lower binding energy, then returns to a higher binding energy, stabilizing at -0.15 eV, close to its initial value. The formation of the metastable phase within some hundreds of femtoseconds after photoexcitation, as evidenced by the concurrent stabilization

of the UHB, LHB, M band energies, together with the B_2 band dispersion, points to an ultrafast switching mechanism in $1T$-TaS_2.

The emergence of the M band within a few tens of femtoseconds following optical excitation, along with its persistence in the metastable phase, points to several possible scenarios outlined below. The first possible scenario is the following. This dispersive band with a minimum at ~ -0.1 eV, closely resembles the band structure around Γ above E_F of the unreconstructed lattice [33,44]. Such a similarity suggests that a metallic phase, characteristic of the unreconstructed lattice, forms immediately after photoexcitation and coexists with the insulating phase in the metastable state, pointing towards phase coexistence. The presence of the Mott phase beyond 700 fs implies that the metastable lattice configuration retains long-range order, with localized energy states confined to the SOD centers, suggesting that a specific PLD in the commensurate CDW phase remains stabilized until long time delays. This is consistent with the equilibrium behavior in $1T$-TaS_2, where the Mott insulating state emerges only if the PLD of the commensurate CDW phase meets the Mott criterion [51,52]. However, from Fig. 2, the PLD is relaxed compared to its equilibrium configuration, suggesting a consequent reduction of the CDW amplitude. Nevertheless, the simultaneous presence of a metallic phase appears inconsistent with the intralayer long-range electronic and lattice order. The lattice may therefore be interpreted as consisting of C-CDW domains with low CDW amplitude separated by metallic regions lacking PLD. Our findings further suggest that the domainlike configuration in the metastable phase differs from the equilibrium NC-CDW and trigonal phases [40,45], which also exhibit domainlike patterns (180–350 K). First, the dispersion of the B_2 band in the metastable (4 ps) and equilibrium (300 K) phases shows significant differences, as seen in Fig. 2. Second, while no LHB is observed at 300 K in equilibrium [45], the Hubbard bands are prominent in the metastable phase, as shown in Fig. 3.

Related forms of phase coexistence with domainlike lattice configurations have been reported in $1T$-TaS_2, though with different characteristics. Recent STM (scanning tunneling microscopy) studies observed metastable phases induced by voltage pulses, revealing a mosaiclike structure of C-CDW domains separated by a disordered network of domain walls, with clear phase shifts between adjacent domains [34,35]. In contrast, x-ray diffraction experiments identified a photo-induced metastable phase featuring C-CDW domains separated by a highly ordered, long-range network of discommensurations. Such a phase was interpreted as a quenched form of NC-CDW phase [33]. The discrepancies between these metastable phases were attributed to surface-bulk effects. However, if phase coexistence picture were the correct explanation for our results, one would also expect to observe the unreconstructed band structure along $\bar{M} \rightarrow \bar{K}$, i.e., a near-parabolic dispersion crossing E_F. But, our data along $\bar{M} \rightarrow \bar{K}$ reveal no such feature, apart from the B_2 band associated with the CDW-reconstructed insulating phase. This indicates that the phase coexistence scenario cannot fully account for our observations.

Another possible scenario is that the M band corresponds to other unoccupied states of the equilibrium insulating phase that undergo independent pump-induced renormalization, rather than representing a feature intrinsic to the metastable phase. If this were the case, the band should also be observable at low pump fluences below the critical value. However, this is not observed: time-resolved spectra for fluences $< F_C$ reveal no additional features above E_F, besides the upper Hubbard band. This rules out the interpretation of the M band as part of the equilibrium band structure, suggesting that it may instead have a different origin.

We now turn to the scenario most consistent with our results. As noted earlier, the M band is absent at fluences below F_C. Immediately above F_C, it is still not observed; however, at fluences $\geqslant 2F_C$, it emerges prominently within 50 fs. Due to reduction in its spectral intensity with time, the band cannot be reliably tracked beyond $\sim$500 fs. For fluences $\geqslant 4$ mJ/cm^2, however, the M band remains observable at longer time delays, when the material has stabilized into the metastable phase. These indicate that the M band is a feature unique to the nonequilibrium band structure, representing a distinct band that only forms under strong photoexcitation. Its appearence only above F_C and persistance till longer times at fluences $\geqslant 3F_C$, identify it as a defining characteristic of the metastable phase. Consequently, the metastable band structure comprises not only the renormalized Hubbard and B_2 bands, but also a distinct new band. This finding is particularly compelling and motivates further studies to probe the structural dynamics of the metastable phase and to elucidate the interactions underlying the emergence of the novel electronic structure. A detailed investigation of the time-dependent behavior of the lower and upper Hubbard bands, including the associated timescales, is underway and may provide critical insight into one of the most debated questions in $1T$-TaS_2: whether the band gap originates primarily from strong electron correlations or from interlayer dimerization.

B. Optical control of the metastable phase

After demonstrating the formation of a metastable phase in $1T$-TaS_2 and outlining its key characteristics, we now investigate how the properties of this phase can be optically manipulated. Tr-ARPES measurements were conducted as a function of pump fluence in the C-CDW phase. The dynamical behavior of the B_2 band will serve as the spectroscopic indicator for optical control.

1. Critical photoexcitation strength for metastable phase

Focusing on the long-time dynamics, we examine the results for band renormalization at 10 ps. From the ARPES spectra in Fig. 4(a), no band renormalization is observed at 10 ps for a low pump fluence of 0.7 mJ/cm^2. In contrast, the ARPES data in Fig. 4(b) shows significant band renormalization at a fluence of 3.4 mJ/cm^2. These differences are clearly reflected in the corresponding E vs $k_\parallel$ dispersions in Fig. 4(c), indicating that weak photoexcitation suppresses the formation of the metastable phase, while strong photoexcitation induces its emergence. This fluence-dependent behavior suggests the existence of a threshold fluence for triggering the metastable phase. To determine this critical fluence, we compared the renormalized bandwidth at 10 ps for different fluences in Fig. 4(d). While the

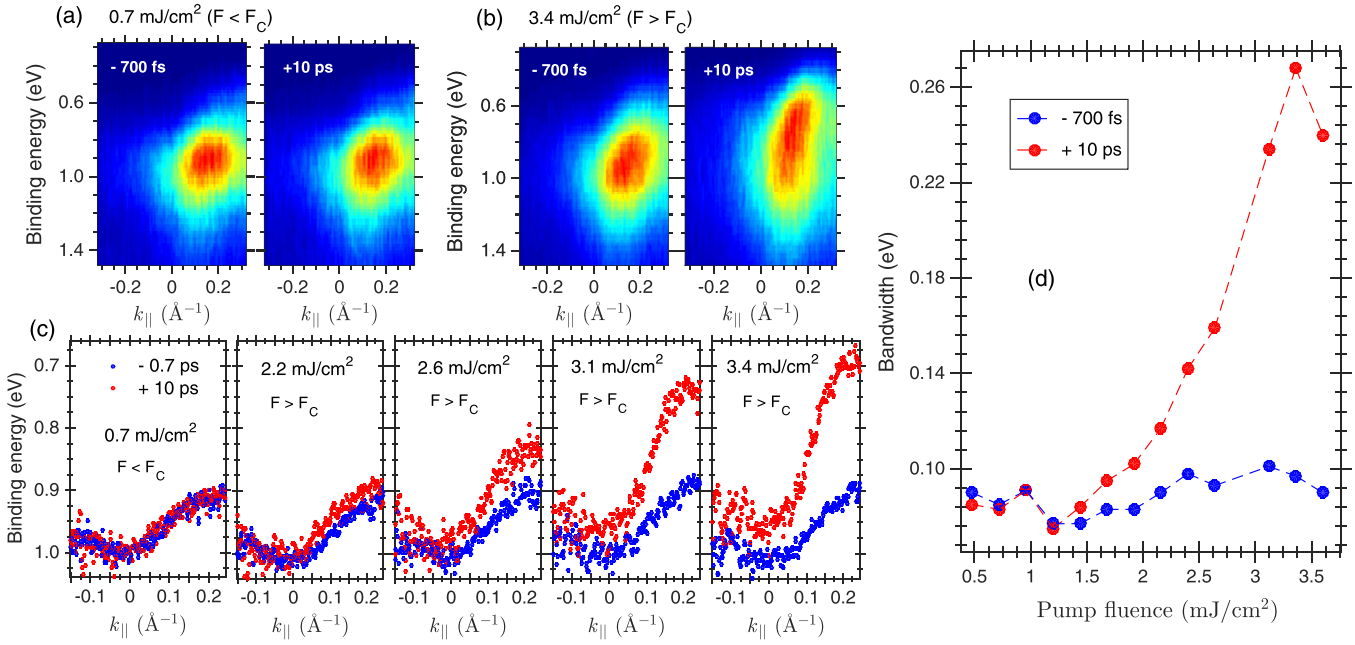

FIG. 4. Critical pump fluence for the metastable phase [B_2 band along $\bar{K} \leftarrow \bar{M} \rightarrow \bar{K}$ ($\bar{M}$ at $k_\parallel = 0$)]: (a) ARPES spectra in equilibrium (left) and at 10 ps (right) for low pump fluence of 0.7 mJ/cm^2 ($< F_C$), acquired using *s*-polarized probe pulses. (b) Same as in (a) at high pump fluence of 3.4 mJ/cm^2 ($> F_C$). (c) E vs $k_\parallel$ dispersion in equilibrium and at 10 ps for different fluences below and above F_C, showing an increase in bandwidth and shift of the band to lower binding energy. (d) Evolution of the bandwidth at 10 ps as a function of pump fluence, identifying a critical fluence $F_C \sim 1.3$ mJ/cm^2. The bandwidth values are accurate within ±8 meV.

equilibrium bandwidth remains independent of fluence, as expected, the bandwidth at 10 ps shows clear differences. For fluences $\leqslant$ 1.3mJ/cm^2, no band renormalization is observed. However, for fluences above this threshold, the dispersion is characterized by an increased bandwidth and a shift to lower binding energy. Thus, we identify a critical incident fluence, $F_C \sim 1.3$mJ/cm^2, corresponding to an absorbed critical fluence $F_C^{ab} \sim 0.7$ mJ/cm^2 (see Experimental Details), associated with the onset of the metastable phase.

Furthermore, the evolution of this phase as a function of fluence reveals important insights. As shown in Figs. 4(c) and 4(d), the degree of band renormalization progressively increases for fluences exceeding F_C. Given that band renormalization serves as a spectroscopic indicator of the metastable phase, this observation implies that the induced metastability can be systematically tuned by varying the photoexcitation strength. On a microscopic level, the observed increase in bandwidth beyond F_C suggests a more pronounced relaxation of the PLD and a concomitant reduction in the CDW amplitude as the density of photoexcited carriers increases.

2. Detailed fluence-dependent dynamics with connection to the transient phase(s)

To further explore the fluence dependence of the metastable phase, we now examine how the nature of the transient phase evolves with fluence and influences the properties of the optically tunable metastable phase. The ARPES spectra in Figs. 5(a) and 5(b) compare the maximum band renormalization at 350 fs for fluences below and above F_C. At 1 mJ/cm^2 ($< F_C$), the renormalization is minimal, suggesting weak transient relaxation of the PLD. In contrast, at 3.7 mJ/cm^2 ($> F_C$), the renormalization is significantly more pronounced, indicating substantial PLD relaxation. Figures 5(c) and 5(d) present the full temporal evolution of the band parameters across different fluences. Following photoexcitation, all fluences exhibit a time-dependent increase in bandwidth and a bandshift towards lower binding energy, followed by a recovery phase after ~350 fs. A common characteristic across all fluences is the structural timescale of 200 fs, which defines the peak transient modifications. This highlights that the transient dynamics are governed by the lattice order, regardless of whether the system ultimately returns to the ground state or transitions into the metastable phase. For fluences below F_C in Figs. 5(c(i)) and 5(d(i)), the PLD undergoes only minimal relaxation, allowing the band renormalization to fully recover within a few picoseconds. In contrast, for fluences exceeding F_C in Figs. 5(c(iii–vi)) and 5(d(iii–vi)), significant PLD relaxation prevents complete recovery, leading to the formation of a metastable phase. This is evidenced by the stabilization of band parameters at different values after 700 fs for all fluences above F_C. Moreover, the transient lattice configuration evolves with fluence, as reflected in the increase of peak band parameter values with fluence. Additionally, the different values of stabilized band parameters increase with fluence above F_C. These suggest that the degree of transient PLD relaxation scales with photoexcitation strength, directly influencing the metastable CDW lattice order. A schematic illustrating the fluence-dependent enhancement of PLD relaxation is shown in Fig. 5(e). For clarity, a single SOD is depicted rather than the entire lattice, which is sufficient since the same dynamics apply uniformly to all SODs throughout the lattice. The existence of a critical fluence of 1.3 mJ/cm^2 and the optically tunable metastable phase is further supported

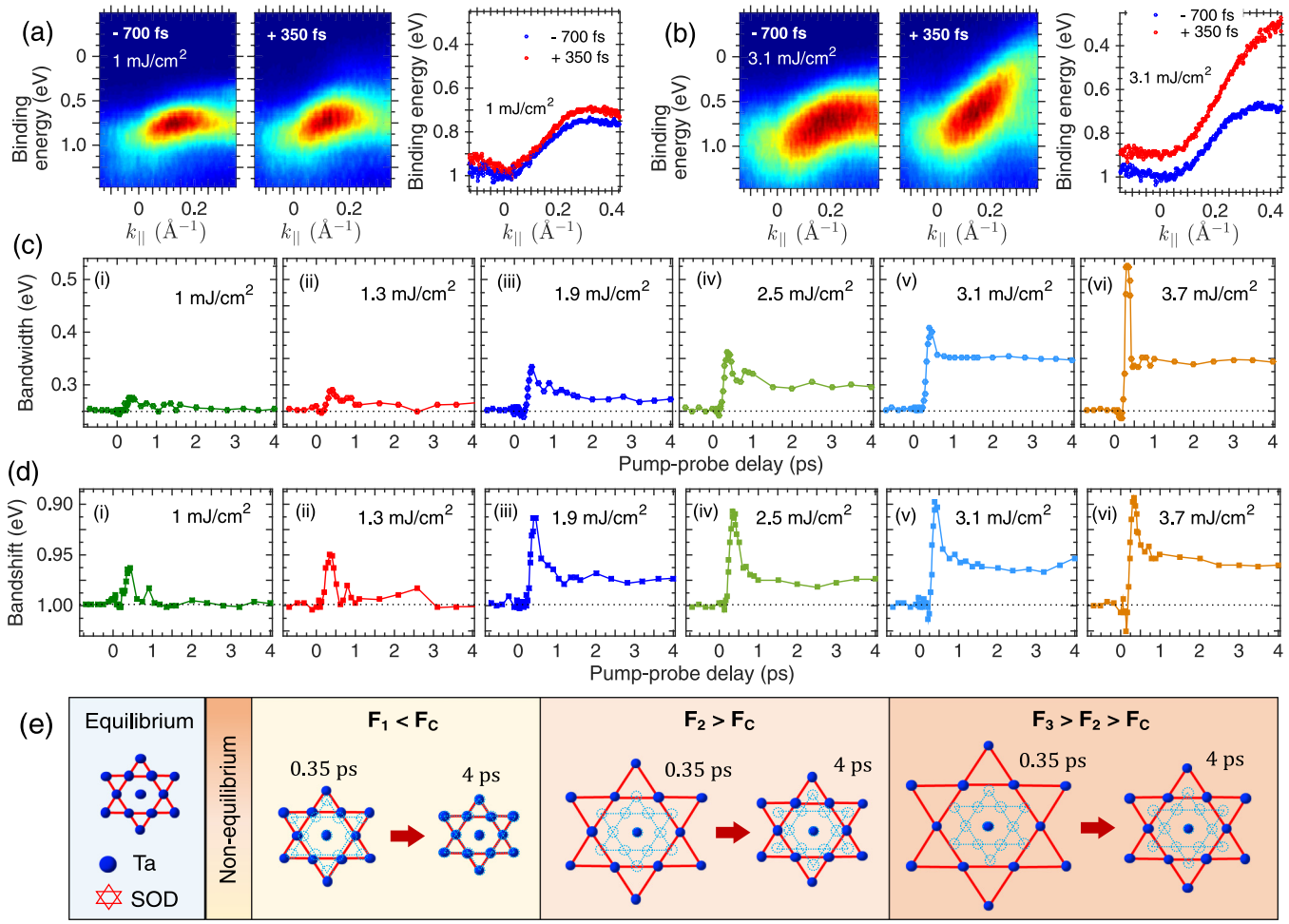

FIG. 5. Optical control of the metastable phase [B_2 band along $\bar{K} \leftarrow \bar{M} \rightarrow \bar{K}$ ($\bar{M}$ at $k_\parallel = 0$)]: (a), (b) ARPES spectra in equilbrium (left) and at 350 fs (right) acquired using *s*-polarized probe pulses, for fluences 1 mJ/cm^2 $< F_C$ and 3.7 mJ/cm^2 $> F_C$, with corresponding E vs $k_\parallel$ dispersion, respectively. (c), (d) Time evolution of bandwidth and bandshift at different pump fluences above and below F_C, suggesting a manipulation of the metastable phase via photoexcitation strength. The bandwidth and bandshift values are accurate within ± 8 and ± 4 meV, respectively. (e) Schematic showing the fluence-dependent modification of periodic lattice distortion. A Star-of-David cluster is used for representation, where dashed lines denote the equilibrium SOD configurations in each case and the ionic displacements are exaggerated for demonstration purposes. F_1, F_2, and F_3 indicate different pump fluences, while F_C is the critical fluence.

by the renormalization of the CDW-derived band at binding energy ~0.5 eV (not shown). In Fig. 6, the time-resolved spectral intensity at 0.8 mJ/cm^2 ($< F_C$) and 1.7 mJ/cm^2 ($> F_C$) exhibits oscillations that correspond to coherent phonons at $\approx$ 2.5 THz, indicative of the excitation of the CDW amplitude mode. The persistence of this mode in the metastable phase suggests that the intrinsic CDW order is maintained despite optical manipulation. This scenario is further supported by the 200 fs timescale associated with the transient dynamics. The pronounced time-periodic modulation of the photoemission intensity points to mode-selective electron-phonon coupling [20], in which only the coupled phonon modes are populated rather than the entire phonon bath. This further excludes lattice heating as the driving mechanism for the metastable phase.

Finally, the metastable phase investigated here is distinct from the previously reported persistent or hidden phases in 1T-TaS_2. Its most notable feature is the emergence of a new

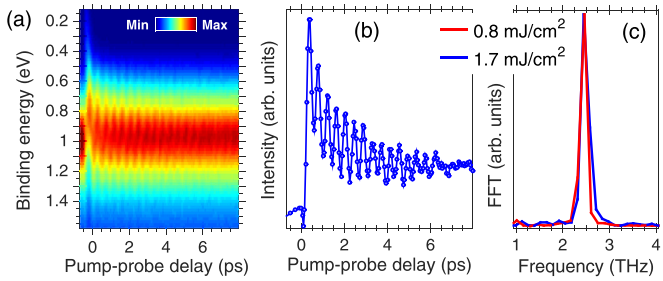

FIG. 6. Coherent phonons: (*s*-polarized probe) (a) Momentum-integrated spectral intensity as a function of binding energy and pump-probe delay, strongly modulated by coherent phonon oscillations. The incident pump fluence is 1.7 mJ/cm^2. (b) Evolution of energy-integrated intensity with time, obtained from (a). (c) Corresponding Fourier transform obtained from (b) after subtracting an exponential decay function. At fluences below and above F_C, the FFT exhibits an intense peak at 2.5 THz for the CDW amplitude mode.

band above E_F, giving rise to a novel band structure not observed in earlier studies. Among the proposed scenarios for the M band, domainlike phase coexistence properties also differ from prior work [22,34,35]. While Maklar *et al.* attributed their hidden phase to an overshoot in ionic displacement producing an inverted CDW geometry [38], we find no evidence of such inverted patterns. In a related CDW system $1T$-$TaSe_2$[20], formation of a metastable phase above a critical fluence is linked to mode-selective electron–phonon coupling, which could be a potential microscopic mechanism for the metastable phase reported in our work.

IV. CONCLUSION

In summary, we demonstrated optical control of a light-induced metastable phase in the C-CDW Mott insulator $1T$-TaS_2 using time-resolved ARPES. By disentangling the independent dynamics of electronic correlations and CDW order, we show that strong photoexcitation induces a long-lived metastable phase. The observed band-structure renormalization reflects a relaxed PLD governed by lattice-driven dynamics, while the emergence of a distinct additional band plausibly indicates the formation of a novel electronic structure unique to the coupled electronic and lattice configuration of the metastable phase. This phase is distinct from thermally accessible equilibrium phases and can only be achieved via optical excitation. To reveal precise control of the metastable phase, we investigated the band renormalization dynamics of a CDW-derived Ta subband as a function of photoexcitation density. We identified a critical pump fluence of 1.3 mJ/cm^2 required to induce the metastable phase. As fluence increases, the phase shifts to higher energies with a progressively relaxed PLD, while the intrinsic CDW amplitude mode remains unaffected. The light-induced lattice distortion within a 200 fs timescale critically determines the stability and characteristics of the metastable phase at each fluence. Our findings offer key insights into the emergence of metastable quantum phases and their ultrafast manipulation, paving the way for controlled optical tuning of correlated electron systems.

ACKNOWLEDGMENTS

We are thankful to E. Nicolini and G. Bortoletto for sample characterization using Laue diffraction. T.S. wishes to express her sincere gratitude to Uwe Bovensiepen for the insightful and illuminating discussions. This research project has received funding from the EU's H2020 framework programme for research and innovation under Grant Agreement No. 101007417 Nanoscience Foundries and Fine Analysis NFFA-Europe-Pilot for the access to the CITIUS facility at the University of Nova Gorica under ID545. This work was funded by the Deutsche Forschungsgemeinschaft (DFG, German Research Foundation) through Project No. 278162697 (SFB 1242).

DATA AVAILABILITY

The data that support the findings of this article are not publicly available because of legal restrictions preventing unrestricted public distribution. The data are available from the authors upon reasonable request.

[1] J. Zhang and R. D. Averitt, Dynamics and control in complex transition metal oxides, Annu. Rev. Mater. Res. **44**, 19 (2014).

[2] D. N. Basov, R. D. Averitt, and D. Hsieh, Towards properties on demand in quantum materials, Nat. Mater. **16**, 1077 (2017).

[3] M. Mitrano, A. Cantaluppi, D. Nicoletti, S. Kaiser, A. Perucchi, S. Lupi, P. Di Pietro, D. Pontiroli, M. Riccò, S. R. Clark, and A. Cavalleri, Possible light-induced superconductivity in K_3C_{60} at high temperature, Nature (London) **530**, 461 (2016).

[4] D. Fausti, R. I. Tobey, N. Dean, S. Kaiser, A. Dienst, M. C. Hoffmann, S. Pyon, T. Takayama, H. Takagi, and A. Cavalleri, Light-induced superconductivity in a stripe-ordered cuprate, Science **331**, 189 (2011).

[5] K. A. Cremin, J. Zhang, C. C. Homes, G. D. Gu, Z. Sun, M. M. Fogler, A. J. Millis, D. N. Basov, and R. D. Averitt, Photoenhanced metastable c-axis electrodynamics in stripe-ordered cuprate $La_{1.885}Ba_{0.115}CuO_4$, Proc. Natl. Acad. Sci. USA **116**, 19875 (2019).

[6] M. Först, C. Manzoni, S. Kaiser, Y. Tomioka, Y. Tokura, R. Merlin, and A. Cavalleri, Nonlinear phononics as an ultrafast route to lattice control, Nat. Phys. **7**, 854 (2011).

[7] T. F. Nova, A. Cartella, A. Cantaluppi, M. Forst, D. Bossini, R. V. Mikhaylovskiy, A. V. Kimel, R. Merlin, and A. Cavalleri, An effective magnetic field from optically driven phonons, Nat. Phys. **13**, 132 (2017).

[8] X. Li, T. Qiu, J. Zhang, E. Baldini, J. Lu, A. M. Rappe, and K. A. Nelson, Terahertz field-induced ferroelectricity in quantum paraelectric $SrTiO_3$, Science **364**, 1079 (2019).

[9] Y. H. Wang, H. Steinberg, P. Jarillo-Herrero, and N. Gedik, Observation of Floquet-Bloch states on the surface of a topological insulator, Science **342**, 453 (2013).

[10] F. Mahmood, C.-K. Chan, Z. Alpichshev, D. Gardner, Y. Lee, P. A. Lee, and N. Gedik, Selective scattering between Floquet-Bloch and Volkov states in a topological insulator, Nat. Phys. **12**, 306 (2016).

[11] A. de la Torre, D. M. Kennes, M. Claassen, S. Gerber, J. W. McIver, and M. A. Sentef, Nonthermal pathways to ultrafast control in quantum materials, Rev. Mod. Phys. **93**, 041002 (2021).

[12] C. L. Smallwood, J. P. Hinton, C. Jozwiak, W. Zhang, J. D. Koralek, H. Eisaki, D.-H. Lee, J. Orenstein, and A. Lanzara, Tracking Cooper pairs in a cuprate superconductor by ultrafast angle-resolved photoemission, Science **336**, 1137 (2012).

[13] J. G. Horstmann, H. Böckmann, B. Wit, F. Kurtz, G. Storeck, and C. Ropers, Coherent control of a surface structural phase transition, Nature (London) **583**, 232 (2020).

[14] K. M. Siddiqui, D. B. Durham, F. Cropp, C. Ophus, S. Rajpurohit, Y. Zhu, J. D. Carlström, C. Stavrakas, Z. Mao, A. Raja, P. Musumeci, L. Z. Tan, A. M. Minor, D. Filippetto, and R. A. Kaindl, Ultrafast optical melting of trimer superstructure in layered 1T'-$TaTe_2$, Commun. Phys. **4**, 152 (2021).

[15] M. Tuniz, D. Soranzio, D. Bidoggia, D. Puntel, W. Bronsch, S. L. Johnson, M. Peressi, F. Parmigiani, and F. Cilento, Ultrafast all-optical manipulation of the charge-density wave in VTe_2, Phys. Rev. Res. **5**, 043276 (2023).

[16] T. Domröse, T. Danz, S. F. Schaible, K. Rossnagel, S. V. Yalunin, and C. Ropers, Light-induced hexatic state in a layered quantum material, Nat. Mater. **22**, 1345 (2023).

[17] H. Mittenzwey, A. M. Kumar, R. Dhingra, K. Watanabe, T. Taniguchi, C. Gahl, K. I. Bolotin, M. Selig, and A. Knorr, Ultrafast optical control of Rashba interactions in a TMDC heterostructure, Phys. Rev. Lett. **134**, 026901 (2025).

[18] V. R. Morrison, R. P. Chatelain, K. L. Tiwari, A. Hendaoui, A. Bruhács, M. Chaker, and B. J. Siwick, A photoinduced metal-like phase of monoclinic VO_2 revealed by ultrafast electron diffraction, Science **346**, 445 (2014).

[19] M. R. Otto, L. P. R. de Cotret, D. A. Valverde-Chavez, K. L. Tiwari, N. Émond, M. Chaker, D. G. Cooke, and B. J. Siwick, How optical excitation controls the structure and properties of vanadium dioxide, Proc. Natl. Acad. Sci. USA **116**, 450 (2019).

[20] X. Shi, W. You, Y. Zhang, Z. Tao, P. M. Oppeneer, X. Wu, R. Thomale, K. Rossnagel, M. Bauer, H. Kapteyn, and M. Murnane, Ultrafast electron calorimetry uncovers a new long-lived metastable state in $1T$-$TaSe_2$ mediated by mode-selective electron-phonon coupling, Sci. Adv. **5**, eaav4449 (2019).

[21] J. Zhang, X. Tan, M. Liu, S. W. Teitelbaum, K. W. Post, F. Jin, K. A. Nelson, D. N. Basov, W. Wu, and R. D. Averitt, Cooperative photoinduced metastable phase control in strained manganite films, Nat. Mater. **15**, 956 (2016).

[22] L. Stojchevska, I. Vaskivskyi, T. Mertelj, P. Kusar, D. Svetin, S. Brazovskii, and D. Mihailovic, Ultrafast switching to a stable hidden quantum state in an electronic crystal, Science **344**, 177 (2014).

[23] A. S. McLeod, J. Zhang, M. Q. Gu, F. Jin, G. Zhang, K. W. Post, X. G. Zhao, A. J. Millis, W. B. Wu, J. M. Rondinelli, R. D. Averitt, and D. N. Basov, Multi-messenger nanoprobes of hidden magnetism in a strained manganite, Nat. Mater. **19**, 397 (2020).

[24] Q. M. Liu, D. Wu, Z. A. Li, L. Y. Shi, Z. X. Wang, S. J. Zhang, T. Lin, T. C. Hu, H. F. Tian, J. Q. Li, T. Dong, and N. L. Wang, Photoinduced multistage phase transitions in Ta_2NiSe_5, Nat. Commun. **12**, 2050 (2021).

[25] D. Mihailovic, D. Svetin, I. Vaskivskyi, R. Venturini, B. Lipovšek, and A. Mraz, Ultrafast non-thermal and thermal switching in charge configuration memory devices based on $1T$-TaS_2, Appl. Phys. Lett. **119**, 013106 (2021).

[26] A. Milloch, M. Fabrizio, and C. Giannetti, Mott materials: Unsuccessful metals with a bright future, npj Spintronics **2**, 49 (2024).

[27] M. Budden, T. Gebert, M. Buzzi, G. Jotzu, E. Wang, T. Matsuyama, G. Meier, Y. Laplace, D. Pontiroli, M. Riccò, F. Schlawin, D. Jaksch, and A. Cavalleri, Evidence for metastable photo-induced superconductivity in K_3C_{60}, Nat. Phys. **17**, 611 (2021).

[28] I. Vaskivskyi, J. Gospodaric, S. Brazovskii, D. Svetin, P. Sutar, E. Goreshnik, I. A. Mihailovic, T. Mertelj, and D. Mihailovic, Controlling the metal-to-insulator relaxation of the metastable hidden quantum state in 1T-TaS_2, Sci. Adv. **1**, e1500168 (2015).

[29] I. Vaskivskyi, I. A. Mihailovic, S. Brazovskii, J. Gospodaric, T. Mertelj, D. Svetin, P. Sutar, and D. Mihailovic, Fast electronic resistance switching involving hidden charge density wave states, Nat. Commun. **7**, 11442 (2016).

[30] J. Ravnik, M. Diego, Y. Gerasimenko, Y. Vaskivskyi, I. Vaskivskyi, T. Mertelj, J. Vodeb, and D. Mihailovic, A time-domain phase diagram of metastable states in a charge ordered quantum material, Nat. Commun. **12**, 2323 (2021).

[31] Y. A. Gerasimenko, P. Karpov, I. Vaskivskyi, S. Brazovskii, and D. Mihailovic, Intertwined chiral charge orders and topological stabilization of the light-induced state of a prototypical transition metal dichalcogenide, npj Quantum Mater. **4**, 32 (2019).

[32] K. Sun, S. Sun, C. Zhu, H. Tian, H. Yang, and J. Li, Hidden CDW states and insulator-to-metal transition after a pulsed femtosecond laser excitation in layered chalcogenide $1T$-$TaS_{1-x}Se_x$, Sci. Adv. **4**, eaas9660 (2018).

[33] Q. Stahl, M. Kusch, F. Heinsch, G. Garbarino, N. Kretzschmar, K. Hanff, K. Rossnagel, J. Geck, and T. Ritschel, Collapse of layer dimerization in the photo-induced hidden state of 1T-TaS_2, Nat. Commun. **11**, 1247 (2020).

[34] L. Ma, C. Ye, Y. Yu, X. F. Lu, X. Niu, S. Kim, D. Feng, D. Tománek, Y.-W. Son, X. H. Chen, and Y. Zhang, A metallic mosaic phase and the origin of Mott-insulating state in 1T-TaS_2, Nat. Commun. **7**, 10956 (2016).

[35] D. Cho, S. Cheon, K.-S. Kim, S.-H. Lee, Y.-H. Cho, S.-W. Cheong, and H. W. Yeom, Nanoscale manipulation of the Mott insulating state coupled to charge order in $1T$-TaS_2, Nat. Commun. **7**, 10453 (2016).

[36] J. Ravnik, I. Vaskivskyi, T. Mertelj, and D. Mihailovic, Real-time observation of the coherent transition to a metastable emergent state in $1T$-TaS_2, Phys. Rev. B **97**, 075304 (2018).

[37] F. Y. Gao, Z. Zhang, Z. Sun, L. Ye, Y.-H. Cheng, Z.-J. Liu, J. G. Checkelsky, E. Baldini, and K. A. Nelson, Snapshots of a light-induced metastable hidden phase driven by the collapse of charge order, Sci. Adv. **8**, eabp9076 (2022).

[38] J. Maklar, J. Sarkar, S. Dong, Y. A. Gerasimenko, T. Pincelli, S. Beaulieu, P. S. Kirchmann, J. A. Sobota, S. Yang, D. Leuenberger, R. G. Moore, Z.-X. Shen, M. Wolf, D. Mihailovic, R. Ernstorfer, and L. Rettig, Coherent light control of a metastable hidden state, Sci. Adv. **9**, eadi4661 (2023).

[39] C. J. Butler, M. Yoshida, T. Hanaguri, and Y. Iwasa, Mottness versus unit-cell doubling as the driver of the insulating state in $1T$-TaS_2, Nat. Commun. **11**, 2477 (2020).

[40] C. B. Scruby, P. M. Williams, and G. S. Parry, The role of charge density waves in structural transformations of $1T$-TaS_2, Philos. Mag. **31**, 255 (1975).

[41] R. H. Friend and A. D. Yoffe, Electronic properties of intercalation complexes of the transition-metal dichalcogenides, Adv. Phys. **36**, 1 (1987).

[42] J. A. Wilson, F. J. D. Salvo, and S. Mahajan, Charge-density waves and superlattices in the metallic layered transition-metal dichalcogenides, Adv. Phys. **24**, 117 (1975).

[43] N. V. Smith, S. D. Kevan, and F. J. D. Salvo, Band structures of the layer compounds 1T-TaS_2 and 2H-$TaSe_2$ in the presence of commensurate charge-density waves, J. Phys. C **18**, 3175 (1985).

[44] K. Rossnagel and N. V. Smith, Spin-orbit coupling in the band structure of reconstructed $1T$-TaS_2, Phys. Rev. B **73**, 073106 (2006).

[45] Y. D. Wang, W. L. Yao, Z. M. Xin, T. T. Han, Z. G. Wang, L. Chen, C. Cai, Y. Li, and Y. Zhang, Band insulator to Mott insulator transition in $1T$-TaS_2, Nat. Commun. **11**, 4215 (2020).

[46] P. Fazekas and E. Tosatti, Electrical, structural and magnetic properties of pure and doped $1T$-TaS_2, Philos. Mag. B **39**, 229 (1979).

[47] W. Wang, D. Dietzel, and A. Schirmeisen, Lattice discontinuities of 1T-TaS_2 across first order charge density wave phase transitions, Sci. Rep. **9**, 7066 (2019).

[48] T. Ritschel, J. Trinckauf, K. Koepernik, B. Buüchner, M. V. Zimmermann, H. Berger, Y. I. Joe, P. Abbamonte, and J. Geck, Orbital textures and charge density waves in transition metal dichalcogenides, Nat. Phys. **11**, 328 (2015).

[49] S.-H. Lee, J. S. Goh, and D. Cho, Origin of the insulating phase and first-order metal-insulator transition in $1T$-TaS_2, Phys. Rev. Lett. **122**, 106404 (2019).

[50] C. W. Nicholson, F. Petocchi, B. Salzmann, C. Witteveen, M. Rumo, G. Kremer, F. O. von Rohr, P. Werner, and C. Monney, Gap collapse and flat band induced by uniaxial strain in $1T$-TaS_2, Phys. Rev. B **109**, 035167 (2024).

[51] L. Perfetti, P. A. Loukakos, M. Lisowski, U. Bovensiepen, M. Wolf, H. Berger, S. Biermann, P. S. Cornaglia, A. Georges, and M. Wolf, Time evolution of the electronic structure of $1T$-TaS_2 through the insulator-metal transition, Phys. Rev. Lett. **97**, 067402 (2006).

[52] L. Perfetti, P. A. Loukakos, M. Lisowski, U. Bovensiepen, M. Wolf, H. Berger, S. Biermann, and A. Georges, Femtosecond dynamics of electronic states in the Mott insulator 1T-TaS_2 by time-resolved photoelectron spectroscopy, New J. Phys. **10**, 053019 (2008).

[53] S. Hellmann, T. Rohwer, M. Kalläne, K. Hanff, C. Sohrt, A. Stange, A. Carr, M. M. Murnane, H. C. Kapteyn, L. Kipp, M. Bauer, and K. Rossnagel, Time-domain classification of charge-density-wave insulators, Nat. Commun. **3**, 1069 (2012).

[54] J. C. Petersen, S. Kaiser, N. Dean, A. Simoncig, H. Y. Liu, A. L. Cavalieri, C. Cacho, I. C. E. Turcu, E. Springate, F. Frassetto, L. Poletto, S. S. Dhesi, H. Berger, and A. Cavalleri, Clocking the melting transition of charge and lattice order in $1T$-TaS_2 with ultrafast extreme-ultraviolet angle-resolved photoemission spectroscopy, Phys. Rev. Lett. **107**, 177402 (2011).

[55] C. Sohrt, A. Stange, M. Bauer, and K. Rossnagel, How fast can a Peierls–Mott insulator be melted? Faraday Discuss. **171**, 243 (2014).

[56] M. Ligges, I. Avigo, D. Golež, H. U. R. Strand, Y. Beyazit, K. Hanff, F. Diekmann, L. Stojchevska, M. Kalläne, P. Zhou, K. Rossnagel, M. Eckstein, P. Werner, and U. Bovensiepen, Ultrafast doublon dynamics in photoexcited $1T$-TaS_2, Phys. Rev. Lett. **120**, 166401 (2018).

[57] T. Saha, A. Pramanik, B. Ressel, A. Ciavardini, F. Frassetto, F. Galdenzi, L. Poletto, A. Ravindran, P. R. Ribič, and G. D. Ninno, Uncovering the nature of transient and metastable nonequilibrium phases in $1T$-TaS_2, Phys. Rev. B **108**, 035157 (2023).

[58] S. Hellmann, M. Beye, C. Sohrt, T. Rohwer, F. Sorgenfrei, H. Redlin, M. Kalläne, M. Marczynski-Bühlow, F. Hennies, M. Bauer, A. Föhlisch, L. Kipp, W. Wurth, and K. Rossnagel, Time-domain classification of charge-density-wave insulators, Phys. Rev. Lett. **105**, 187401 (2010).

[59] M. Eichberger, H. Schäfer, M. Krumova, M. Beyer, J. Demsar, H. Berger, G. Moriena, G. Sciaini, and R. J. Dwayne Miller, Snapshots of cooperative atomic motions in the optical suppression of charge density waves, Nature (London) **468**, 799 (2010).

[60] C. Bao, H. Zhong, F. Wang, T. Lin, H. Zhang, Z. Sun, W. Duan, and S. Zhou, Distinguishing and controlling Mottness in $1T$-TaS_2 by ultrafast light, Phys. Rev. B **107**, L121103 (2023).

[61] C. Grazioli, C. Callegari, A. Ciavardini, M. Coreno, F. Frassetto, D. Gauthier, D. Golob, R. Ivanov, A. Kivimäki, B. Mahieu, B. Bučar, M. Merhar, P. Miotti, L. Poletto, E. Polo, B. Ressel, C. Spezzani, and G. De Ninno, CITIUS: An infrared-extreme ultraviolet light source for fundamental and applied ultrafast science, Rev. Sci. Instrum. **85**, 023104 (2014).

[62] L. Poletto, P. Villoresi, F. Frassetto, F. Calegari, F. Ferrari, M. Lucchini, G. Sansone, and M. Nisoli, Time-delay compensated monochromator for the spectral selection of extreme-ultraviolet high-order laser harmonics, Rev. Sci. Instrum. **80**, 123109 (2009).

[63] J. R. Duffey, R. D. Kirby, and R. V. Coleman, Raman scattering from 1T-TaS_2, Solid State Commun. **20**, 617 (1976).

[64] J. Demsar, L. Forró, H. Berger, and D. Mihailovic, Femtosecond snapshots of gap-forming charge-density-wave correlations in quasi-two-dimensional dichalcogenides $1T$-TaS_2 and $2H$-$TaSe_2$, Phys. Rev. B **66**, 041101(R) (2002).

[65] See Supplemental Material at http://link.aps.org/supplemental/10.1103/gz2s-685y for momentum-resolved EDC stacks along $\bar{K} \leftarrow \bar{M} \rightarrow \bar{K}$ at different temperatures, clearly showing that the bandwidth narrows as the temperature increases.

[66] A. Damascelli, Probing the low-energy electronic structure of complex systems by ARPES, Phys. Scr. **T109**, 61 (2004).

Correction: The omission of a support statement in the Acknowledgments has been fixed.